

Geometry and mechanics of micro-domains in growing bacterial colonies

Zhihong You,¹ Daniel J. G. Pearce,¹ Anupam Sengupta,² and Luca Giomi¹

¹*Instituut-Lorentz, Universiteit Leiden, P.O. Box 9506, 2300 RA Leiden, The Netherlands*

²*Institute for Environmental Engineering, Department of Civil,
Environmental and Geomatic Engineering, ETH Zurich,
Stefano-Franscini-Platz 5, 8093 Zurich, Switzerland*

Bacterial colonies are abundant on living and non-living surfaces and are known to mediate a broad range of processes in ecology, medicine and industry. Although extensively researched, from single cells to demographic scales, a comprehensive biomechanical picture, highlighting the cell-to-colony dynamics, is still lacking. Here, using molecular dynamics simulations and continuous modelling, we investigate the geometrical and mechanical properties of a bacterial colony growing on a substrate with free boundary, and demonstrate that such an expanding colony self-organizes into a “mosaic” of micro-domains consisting of highly aligned cells. The emergence of micro-domains is mediated by two competing forces: the steric forces between neighboring cells which favour cell alignment, and the extensile stresses due to cell growth that tend to reduce the local orientational order, and thereby distort the system. This interplay results into an exponential distribution of the domain areas, and sets a characteristic length scale proportional to the square root of the ratio between the system orientational stiffness and the magnitude of the extensile active stress. Finally, our examination of the internal stresses reveal that, in addition to biochemical pathways, the spatiotemporal organization in microbial colonies is significantly affected by the mechanical forces exerted and experienced by the growing cells.

Bacteria successfully colonize a plethora of surfaces by producing hydrated extracellular polymeric matrix, generally composed of proteins, exopolysaccharides and extracellular DNA [1]. Such surface-associated communities play a crucial role in the pathogenesis of many chronic infections: from benign dental caries in the oral cavity [2, 3] to life-threatening cystic fibrosis and catheter-related endocarditis [4]. In contrast to their planktonic counterpart, comprising freely moving cells (by virtue of swimming, gliding, or swarming motion), cells in a sessile colony lack motility. Since most bacteria found in nature exist predominantly as surface-associated colonies [5], they are permanently exposed to a range of surface-specific forces [6]: time-varying internal stress due to growth, contact forces due to interactions with the neighboring cells and substrate they are growing on, or shear stresses due to ambient flows in the system.

Our understanding of the mechanics of bacterial growth is still at its infancy, specifically in light of the wide range of mechanical cues that single cells overcome to successfully colonize surfaces. Although it has been long known that mechanical forces play a critical role in the development and fitness of eukaryotic cells, and, in addition, can regulate key molecular pathways [10], the cornerstone of major discoveries in bacterial communities have relied on biochemical pathways triggered exclusively by chemical stimuli [11]. It is only recently that the role of mechanics in the ecophysiology of prokaryotic cells is coming to the forefront [6, 12–19], highlighting the governing biophysical principles that drive colony formation.

Here we investigate the spatial organization and the stress distribution of a colony of non-motile, rod shaped bacteria growing on a substrate with free boundary con-

ditions. Although non-motile bacteria interact mostly through steric forces, pushing each other out of the way as they grow in length, the combination of these passive forces with the bacteria active growth results into a complex internal dynamics as well the formation of coherent structures (Fig. 1a-c) reminiscent of those observed in active liquid crystals [20–24]. Using molecular dynamics simulations and continuous modeling, we demonstrate that an expanding colony self-organizes into a “mosaic” of nematic micro-domains, whose typical size is set by the competition between growth-induced active forces, that tend to disorder the system, and passive steric forces, that tend to reorganize the bacteria into close packed nematic structures. This competition results into an exponential distribution of the domain areas, with a characteristic length scale proportional to the square root of the ratio between the system orientational stiffness and the magnitude of the extensile active stress. Both active and passive forces scale linearly with the cell density. Therefore, despite the colony being denser in the center than at the periphery, such an inherent length scale remains uniform throughout the system.

This paper is organized as follows: in Sec. I, we introduce a hard-rod model for growing bacteria and we describe the geometrical (Sec. IA) and mechanical (Sec. IB) properties of the emergent micro-domains. Building on these results, in Sec. II we construct a continuum theory for growing bacterial colonies grounded on the hydrodynamics of active nematic liquid crystals. Finally, in Sec. III, we discuss our results and modelling approach in the context of previously reported experiments, and draw conclusions emphasising the role of geometry and mechanics during the early stages of biofilm formation.

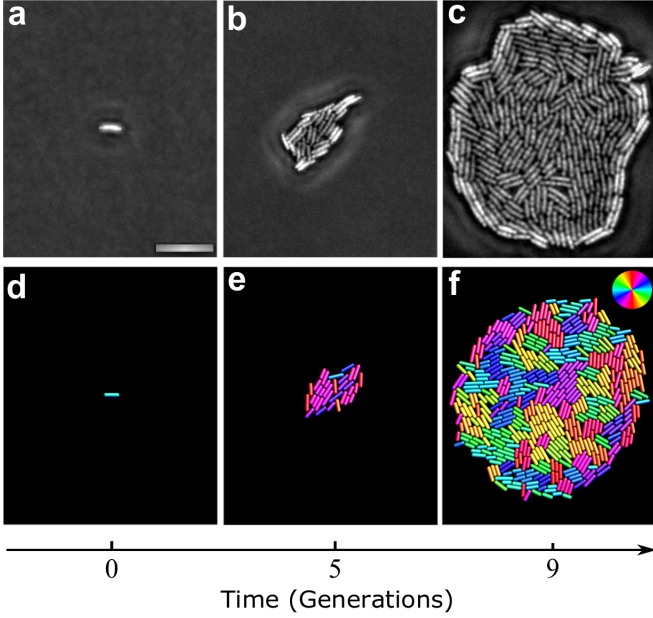


FIG. 1. **Growth of a bacterial colony.** (a)-(c) Phase contrast micrographs at different time points capture the growth of a single cell of non-motile strain of *Escherichia coli* to a two-dimensional colony under free boundary conditions (the cell doubling time is ≈ 32 minutes, and the scale bar corresponds to $2 \mu\text{m}$). Depending upon the physiological state, the aspect ratio of the cells (length/width) varied between 3.1 and 4.5. (d)-(f) The corresponding three time points during the growth of a bacterial colony obtained using molecular dynamics simulations (Sec. I). The rods are colour coded by their orientation as described in the colour wheel (panel f, upper right corner).

I. Hard-rod model

A. Stochastic geometry of bacterial colonies

We model each bacterium as a spherocylinder with a fixed diameter d_0 and a time-dependent length l (excluding the caps on both ends), growing in a two dimensional space [18]. The position, \mathbf{r}_i , and the orientation, $\mathbf{p}_i = (\cos \theta_i, \sin \theta_i)$, of cell i ($i = 1, 2, \dots$), are governed by the over-damped Newton equations for a rigid body, namely:

$$\frac{d\mathbf{r}_i}{dt} = \frac{1}{\gamma l_i} \sum_j \mathbf{F}_{ij}, \quad (1a)$$

$$\frac{d\theta_i}{dt} = \frac{12}{\gamma l_i^3} \sum_j (\mathbf{r}_{ij} \times \mathbf{F}_{ij}) \cdot \hat{\mathbf{z}}, \quad (1b)$$

where γ is a constant drag per unit length and the summation runs over all the cells in contact with the i -th. The points of contact have positions \mathbf{r}_{ij} with respect to the center of mass of the i -th cell and apply Hertzian forces of the form $\mathbf{F}_{ij} = Y d_0^{1/2} h_{ij}^{3/2} \mathbf{N}_{ij}$, where Y is proportional to the Young's modulus, h_{ij} is the overlap distance between the i -th and j -th cells, and \mathbf{N}_{ij} their common normal unit vector. The length l_i increases in

time and, after this reaches the division length l_d , the cell divides into two identical daughter cells. In order to avoid synchronization of divisions, the growth rate of each cell, defined as the length increment per unit time, is randomly chosen from an interval $[g/2, 3g/2]$, where g is the average growth rate. Immediately after duplication, the daughter cells have the same orientation as the mother cell, but independent growth rates. The rate of cell division in a bacterial colony can vary over time, with the increase of growth-induced local pressure [25]. However, such an effect is minimal during the initial stages of colony growth studied here, and hence neglected in our simulations. All our simulations, start from a single randomly orientated cell, which is then free to grow in length and duplicate. We rescale length by d_0 , time by γ/Y , and integrate Eqs. (1) with time step $\Delta t = 10^{-2}$.

Fig. 1 shows the typical configurations observed at the early stages of colonization both *in vitro* and *in silico*. The emergence of local nematic order is conspicuous throughout the system, however this does not propagate across the colony, but remains confined into a set of microscopic domains. These nematic domains, or “patches”, are separated from each other by fracture lines reminiscent of grain boundaries in crystals [26]. As the colony evolves, the domains grow, merge, buckle, and break apart, in a complex sequence of morphological and topological transformations.

Fig. 3 shows three examples of proliferating colonies of cells each with different division length l_d , and hence, different aspect ratios. The typical domain area, as we can see, depends on the length of the cell at division. Overall, the micro-domains have no preferential orientation (insets in Fig. 3), and the colony is globally isotropic and characterized by the circular shape. The absence of the global orientational order can be ascribed to the inherent instability of the domains, that continuously buckle and fracture under the effect of growth-induced stress. The

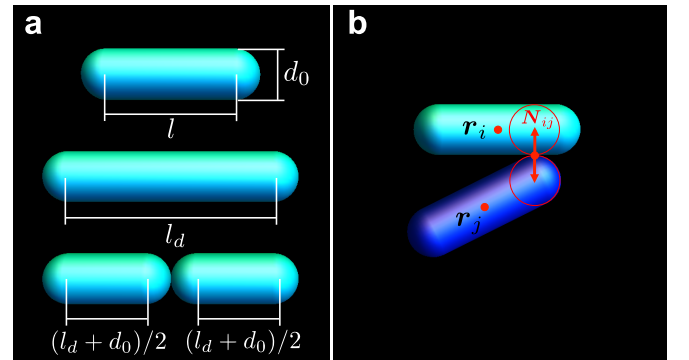


FIG. 2. **Hard-rod model of bacterial growth.** (a) Bacteria are modeled as spherocylinders with a fixed diameter d_0 and time-dependent length. The distance l between the two caps grows linearly in time and, after this reaches the division length l_d , the cell divides into two identical daughter cells. (b) Cell-cell interaction is modeled via Hertzian forces acting along the normal direction \mathbf{N}_{ij} .

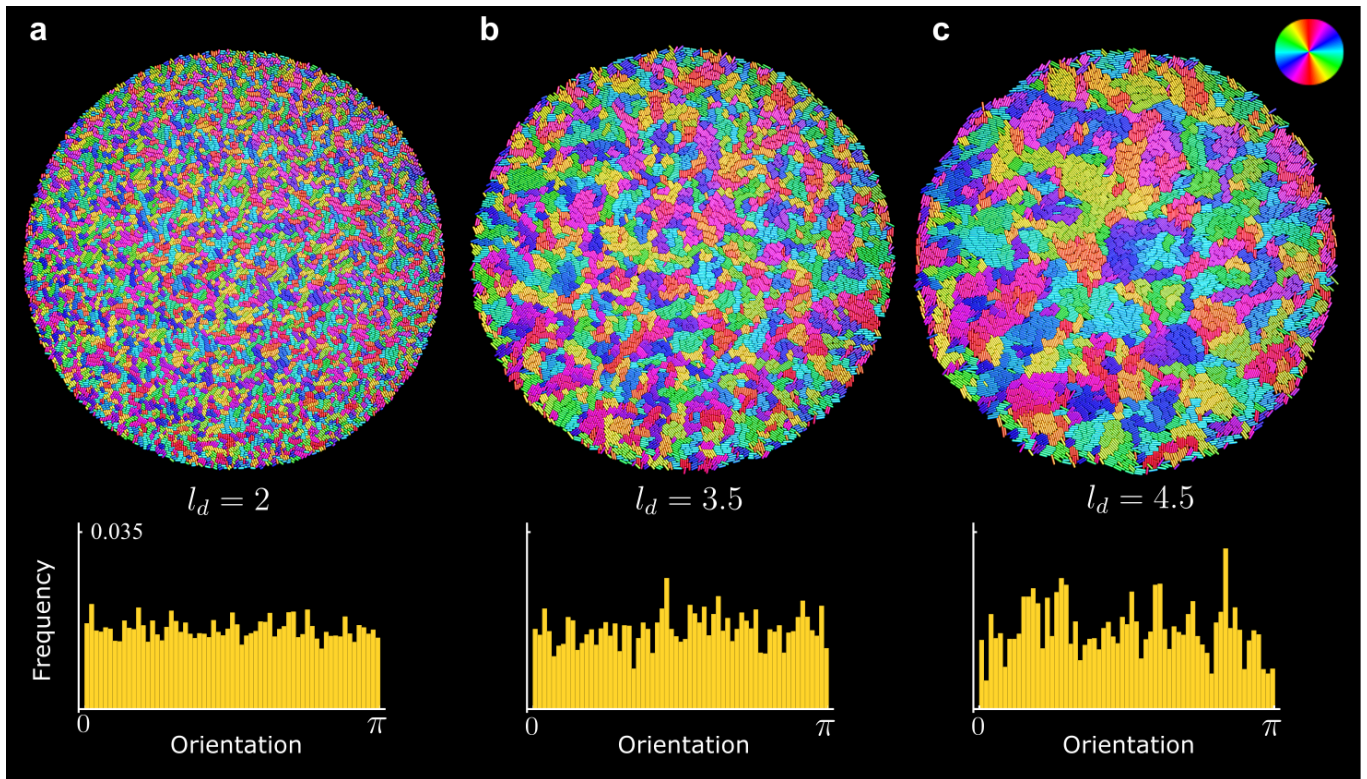


FIG. 3. **Emergence of nematic domains in proliferating bacterial colonies.** (a)-(c) Examples of nematic micro-domains emerging in simulated bacterial colonies for various division lengths ($l_d = 2, 3.5, 4.5$, in units of the cell diameter d_0). Cells are colored by their orientation. Upon increasing the division length, the typical area of the domains increases progressively. Inside a domain, the cells are highly aligned, while there is no preferential orientation at the scale of the entire colony, as confirmed by the probability distribution of cell orientations (insets).

typical domain area then represents not only the coherent length scale of orientational order, but also the length scale at which the colony internal stresses compromise.

To quantify the geometry of the bacterial colonies, we have introduced the following domain segmentation criterion: two cells belong to the same domain if they are in contact, and that their relative orientation differs by less than 3%. As this definition depends on the choice of a threshold, so will the distribution of domain area. Nonetheless, the structure of the distribution and the general trends identified in the various observables, are generally robust and independent of the chosen threshold. A central quantity to characterize the geometry of a colony, is the probability density of the domain area, $P(A)$. Fig. 4a shows a plot of this quantity measured for three colonies with different division lengths. The frequency of domains with area A decreases with A , and for sufficiently large A values, $P(A)$ approaches the exponential distribution:

$$P(A) \sim \exp\left(-\frac{A}{A^*}\right), \quad (2)$$

where A^* is a characteristic area scale proportional depending on the division length l_d and proportional to the typical area of the micro-domains.

In order to quantify the spatial dependence of the domain areas, we have calculated the average domain area restricted to an annular strip located at distance r from the center of the colony, denoted $\langle A \rangle_r$ (Fig. 4a, inset). The local domain area is uniform in the bulk of the colony, for a given aspect ratio of the cells, before dropping to zero at the boundary, where the colony is more disordered. In turn, the average domain area in the bulk $\langle A \rangle$, is strongly affected by the division length l_d . This is visibly conspicuous in Fig. 3. Increasing l_d causes the cells to be, on average, more slender, resulting in larger and more stable domains, as revealed by the plot in Fig. 4b. More interestingly, increasing the growth rate g has the opposite effect, and causes a drop in the domain area (Fig. 4c). The results demonstrate that the emergent geometrical attributes of the micro-domains in a growing bacterial colony are regulated by the competing effects of cell length and the division rate. These effects can ultimately be ascribed to the mechanical properties of the system, as we will explain in the next subsection.

B. Mechanical properties

The domain geometry in a proliferating bacterial colony is determined by the interplay between two competing

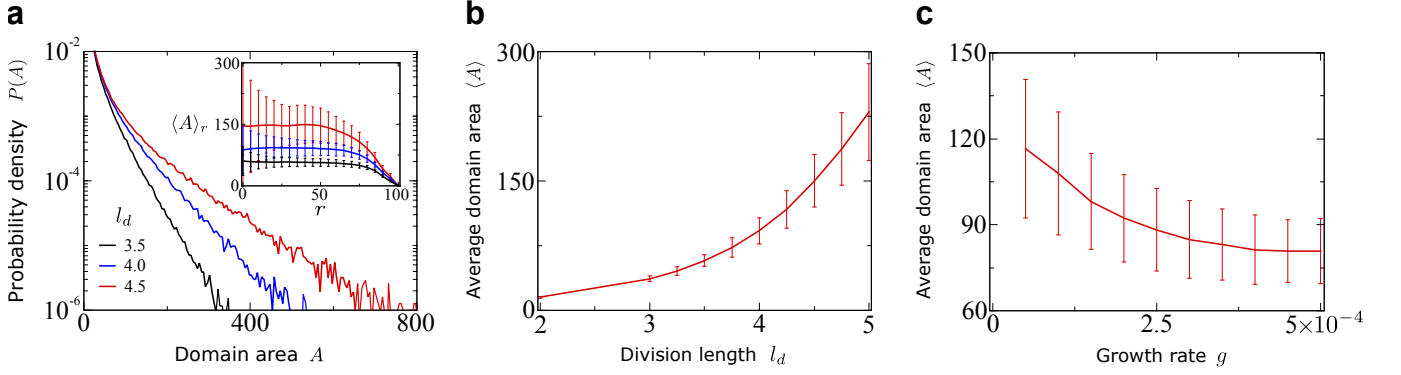


FIG. 4. **Geometry of nematic micro-domains in bacterial colonies.** (a) Probability distributions of domain area, $P(A)$, for various division length l_d . The domain area is exponentially distributed, with a slope that decreases with the division length l_d . (inset) The average domain area at a distance r from the centre of the colony, showing that the area of the domains is approximately constant in the bulk of the colony and drops at the boundary. The bulk domain area $\langle A \rangle$ increases with the division l_d (b) and decreases with the growth rate g (c). $\langle A \rangle$ is calculated by averaging the areas of all domains within the range $0 \leq r \leq R/2$, with R the colony radius. In all results presented, length is expressed in units of the cell width, d_0 , and time in units of the time scale γ/Y defined in Eqs. (1)

forces: steric repulsion between neighboring cells and the extensile stresses due to cell growth. While cell-cell steric repulsion favors alignment, the emergent extensile stresses due to the growth within a restricted environment (i.e., the space delimited by the neighboring domains), tend to deform, and eventually fracture a domain. Both these effects are due to contact forces and are, therefore, enhanced by the local packing fraction, ϕ . To clarify this concept, we have measured the local packing fraction $\phi(r, t) = \sum_i a_i(t)/\mathcal{A}_r$, where $a_i(t)$ is the area of the i -th cell, located at time t inside a thin annulus of radius r and area \mathcal{A}_r , centered at the colony center. As we have found, the colony has a radial symmetry, hence the local packing fraction depends exclusively on the distance r from the center. Fig. 5a shows that at any given time the packing fraction decreases monotonically with r . As bacteria duplicate and progressively colonize the surrounding space, the local packing fraction increases throughout the system while maintaining a characteristic spatial profile that smoothly interpolates between a time-dependent maximum $\phi(0, t) = \phi_{\max}(t)$, at the center of the colony, and the time-independent minimum, $\phi(R, t) = \phi_c$, at the edge (R being the colony radius). The quantity $\phi_c \approx 1$ is the critical packing fraction at which the cells first start to compress each other. In close proximity of the edge of the colony, $\phi < \phi_c$ and the contact forces tend to reorient the cells without compressing them, leading to an abrupt drop in packing fraction. Upon rescaling density by $\phi(0) - \phi(R)$ and distance r by the colony radius R , the density spatial dependence can be described, at any time, by a simple quadratic law:

$$\frac{\phi(r) - \phi(R)}{\phi(0) - \phi(R)} = 1 - \left(\frac{r}{R}\right)^2, \quad (3)$$

as illustrated in the inset of Fig. 5a. As we will analytically prove in Sec. II, such a density profile originates

from balance between growth-induced pressure and drag.

The tendency of the cells to align with each other is driven by the local steric interactions, and can be conceptualized in the framework of Frank elasticity [27], starting from the free-energy density:

$$f_F = \frac{1}{2} k_F |\nabla \mathbf{n}|^2. \quad (4)$$

Here k_F is an orientational stiffness penalizing, in equal amount, splay and bending deformations and \mathbf{n} is the nematic director corresponding to the average orientation of the bacteria. Any departure from the uniformly aligned configuration causes restoring forces proportional to the field $\mathbf{h} = -\delta/\delta \mathbf{n} \int dA f_F = k_F \nabla^2 \mathbf{n}$ [27]. As a consequence of growth, each cell further acts as an extensile force dipole that pushes away its neighbors along the $\pm \mathbf{n}$ direction. This collectively gives rise to an internal stress of the form:

$$\boldsymbol{\sigma} = -p \mathbf{I} + \alpha \left(\mathbf{n} \mathbf{n} - \frac{1}{2} \mathbf{I} \right), \quad (5)$$

where p is the pressure, \mathbf{I} the identity matrix and α the deviatoric active stress [28, 29]. In the most general case, the three quantities k_F , p and α , appearing in Eqs. (4) and (5), are functions of the local packing fraction, and the nematic order parameter, in addition to the cell aspect ratio and the growth rate.

Eqs. (4) and (5) identify a fundamental length scale $\ell_a = \sqrt{k_F/|\alpha|}$, proportional to the length at which the orientational elastic stress balances the extensile active stress [20]. This length scale plays a pivotal role in the mechanics of active fluids, and, depending on how it compares with the system size L , it determines the system mechanical behavior. Active nematics liquid crystals, in particular, relax toward the minimum of the Frank free energy when $\ell_a \gg L$, as the restoring forces arising in

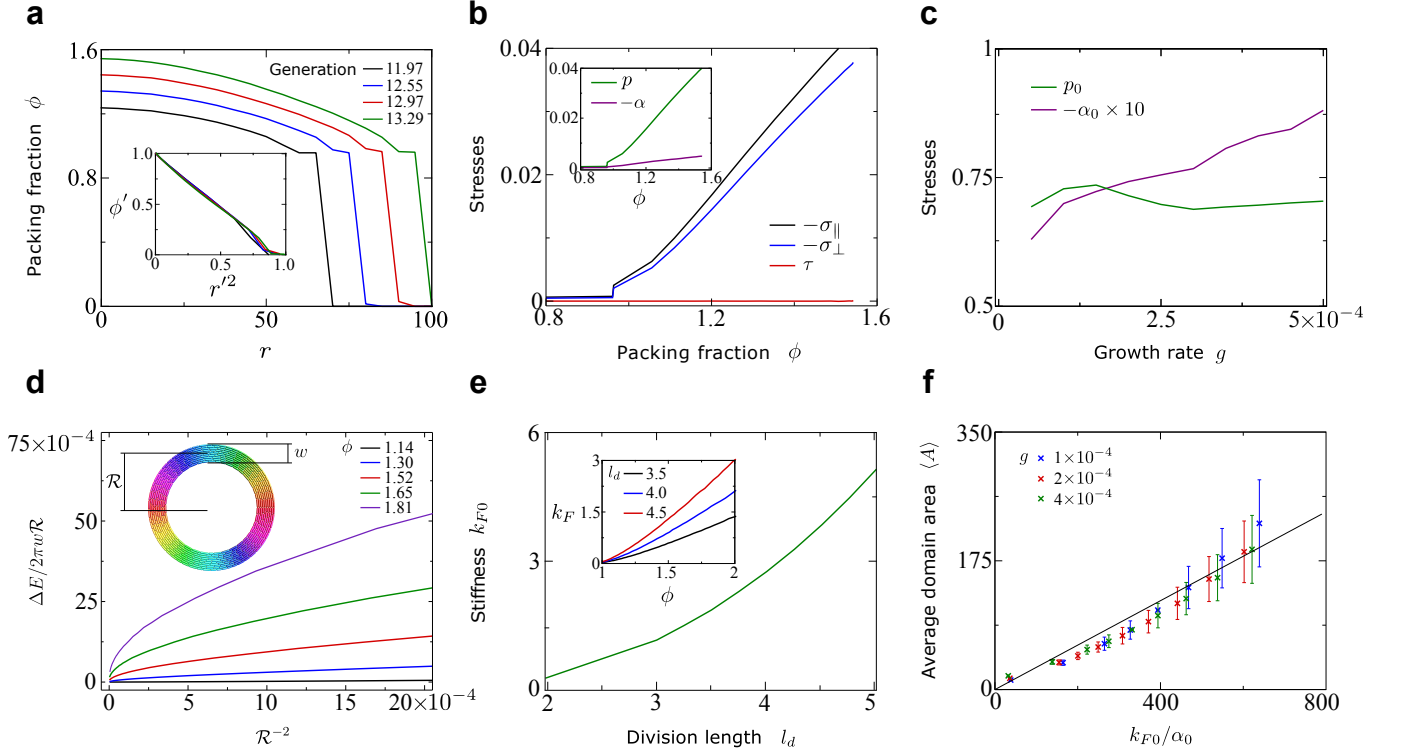


FIG. 5. **Mechanical properties of micro-domains in growing bacterial colonies.** (a) Spatial dependence of packing fraction for different ages of colonies. The inset shows $\phi' = [\phi(r) - \phi(R)]/[\phi(0) - \phi(R)]$ versus $r'^2 = (r/R)^2$. All the curves collapse on the same line as demanded by Eq. (3). (b) Different components of the internal stress σ as functions of packing fraction ϕ . The normal stress parallel to the director \mathbf{n} , σ_{\parallel} , is larger than that perpendicular to it, i.e. σ_{\perp} . Both $|\sigma_{\parallel}|$ and $|\sigma_{\perp}|$ are piecewise linear functions of ϕ , while the shear component τ vanishes. The normal components of stress can be rearranged into a hydrostatic pressure p and an extensile active stress α , both increase linearly with the packing fraction (inset). (c) The pressure is independent of growth rate g , while the active stress increases with it. (d) Difference of energy density (energy per unit area) between the straight channel and a ring-shaped channel of radius R , as a function of R^{-2} . An example of ring-shaped channel is shown in the inset, with radius R and width w . Cells are colored by their orientations as in Fig. 3. (e) The orientational stiffness k_F increases linearly with packing fraction, and the prefactor of the linear fit, k_{F0} , increases with the division length l_d . (f) The averaged domain area $\langle A \rangle$ is approximately proportional to k_{F0}/α_0 , for various combinations of growth rate and division length. We chose three growth rates (identified by colors), and for each growth rate we gradually increase the division length from $l_d = 2$ to $l_d = 5$, corresponding to different data points with the same color. In all results presented, length is expressed in units of the cell width, d_0 , and time in units of the time scale γ/Y defined in Eqs. (1)

response to the elastic distortions outweigh the active forces. As $\ell_a \sim L$, the nematic ground state becomes unstable to a state characterized by a spontaneous distortion and laminar flow [30–34]. Such a steady state becomes unstable to an oscillatory state when $\ell_a < L$ [33, 34], while for $\ell_a \ll L$, the dynamics are completely chaotic [20]. Recent experiments on motile *B. subtilis* under confinement [35], have confirmed this fascinating scenario and opened the way to understanding the effect of environmental stimuli in active materials.

In the following, we demonstrate that in a growing colony of non-motile cells, the inherent length scale ℓ_a determines the geometrical properties of the micro-domains in such a way that $\langle A \rangle \sim \ell_a^2$. For this purpose, we have measured the orientational stiffness k_F and the stresses σ exerted inside the colony. The latter can be calculated

from the virial expansion [13]:

$$\sigma_i = \frac{1}{2a'_i} \sum_j \mathbf{r}_{ij} \mathbf{F}_{ij}, \quad (6)$$

where $a'_i = a_i/\phi$ is the effective area occupied by the i -th cell. Fig. 5b shows a plot of the various components of the stress tensor versus packing fraction, given by Eq. (6). The tensor is expressed in the basis of the nematic director and its normal $\mathbf{n}^{\perp} = (-n_y, n_x)$, namely:

$$\sigma = \sigma_{\parallel} \mathbf{n} \mathbf{n} + \sigma_{\perp} \mathbf{n}^{\perp} \mathbf{n}^{\perp} + \tau \{\mathbf{n}, \mathbf{n}^{\perp}\}, \quad (7)$$

where $\{\cdot, \cdot\}$ denotes the commutator. As expected the normal stresses σ_{\parallel} and σ_{\perp} increases with packing fraction and, at any finite packing fraction, are such that $|\sigma_{\parallel}| > |\sigma_{\perp}|$, as a consequence of the anisotropic cell growth. The shear-stress τ , on the other hand, is always negligible because of the absence of lateral friction

between the cells. Note that both σ_{\parallel} and σ_{\perp} are negative because of the extensile nature of the growth-induced forces. The dependence of the normal stresses on packing fraction is piecewise linear: for $\phi < \phi_c$, the contact forces can be relieved by rotations and repositioning of the cells and $\sigma_{\parallel} \approx \sigma_{\perp} \approx 0$; while for $\phi > \phi_c$, the cells in the bulk are tightly packed and internal stresses build up as the packing fraction increases. Setting $\tau = 0$ in Eq. (7) and taking $\mathbf{n}^{\perp} \mathbf{n}^{\perp} = \mathbf{I} - \mathbf{n} \mathbf{n}$, one can rearrange the stress tensor in the form:

$$\boldsymbol{\sigma} = \frac{\sigma_{\parallel} + \sigma_{\perp}}{2} \mathbf{I} + (\sigma_{\parallel} - \sigma_{\perp}) \left(\mathbf{n} \mathbf{n} - \frac{1}{2} \mathbf{I} \right). \quad (8)$$

Comparing this with Eq. (5), straightforwardly yields $p = (|\sigma_{\parallel} + \sigma_{\perp}|)/2$ and $\alpha = \sigma_{\parallel} - \sigma_{\perp}$. Together with the numerical results summarized in Fig. 5, this implies:

$$p = p_0(\phi - \phi_c), \quad \alpha = -\alpha_0|\phi - \phi_c|, \quad (9)$$

as long as $\phi > \phi_c$. Not unexpectedly, the longitudinal growth of the cells gives rise to an extensile (i.e. $\alpha < 0$) active stress that decreases monotonically with the distance from the center of the colony. The pre-factors p_0 and α_0 are plotted in Fig. 5c as a function of the growth rate g . The active stress α_0 increases monotonically with g , while p_0 is essentially independent.

In order to estimate the orientational stiffness k_F , we place our *in silico* bacterial colony inside an annular channel of width w and radius \mathcal{R} (Fig. 5d, $w \ll \mathcal{R}$), and calculate the energy associated with the Hertzian contacts: $E = (2/5) Y d_0^{1/2} \sum_{\langle ij \rangle} h_{ij}^{5/2}$, where the summation runs over all the pairs of cells in contact with each other. By comparing how the energy density changes with the curvature of the channel we can infer the orientational stiffness. Fig. 5d shows a plot of the difference $\Delta E = E(\phi, \mathcal{R}) - E(\phi, \infty)$ between the energy of bent and a straight (i.e. $\mathcal{R} \rightarrow \infty$) channel, normalized by the area $2\pi w \mathcal{R}$ of the channel, as a function of the squared curvature $\kappa^2 = 1/\mathcal{R}^2$. From Eq. (4) it follows that $k_F = \partial_{\kappa^2} \Delta E / (2\pi w \mathcal{R})|_{\kappa=0}$. As shown in the inset of Fig. 5e, the orientational stiffness k_F increases linearly with packing fraction, i.e. $k_F = k_{F0}(\phi - \phi_c)$. Furthermore, increasing the the slenderness of the cells, makes the colony orientationally stiffer (Fig. 5e).

Combining the measurements of the extensile active stress and the orientational stiffness, we are finally able to formulate a scaling law for the area of the nematic micro-domains comprising our simulated bacterial colonies. Namely:

$$\langle A \rangle \sim \frac{k_F}{|\alpha|}, \quad (10)$$

in agreement with our numerical data (Fig. 5f). In summary, bacterial colonies freely growing on a two-dimensional frictional substrate spontaneously organize into a “mosaic” of micro-domains consisting of highly aligned cells. The domains are randomly oriented so that

the colony is globally isotropic and circularly symmetric at the global scale, while their areas are exponentially distributed, as indicated in Eq. (2). Such a distribution results from the competition between passive steric forces, that favor local alignment, and the extensile active forces originating from the cell growth. These forces balance at the length $\ell_a = \sqrt{k_F/|\alpha|}$, resulting in a characteristic domain area that scales as ℓ_a^2 . Remarkably, both the orientational stiffness k_F and the extensile active stress α scale linearly with the packing fraction ϕ . Consequently $k_F/\alpha = k_{F0}/\alpha_0$, so that and the average domain area is uniform throughout the colony (Fig. 4 inset). Such a peculiar cancellation of the density dependence is presumably specific of the type of interactions chosen here and we do not expect it to hold in general. Including the bending elasticity of the cells could, for instance, change the density dependence of k_F and α , resulting in a space-dependent active length scale. Yet, the mechanism described here and summarized by Eq. (10) is general and does not depend on the details of the model.

II. Continuous model

In this section we demonstrate that much of the behavior previously described can be quantitatively captured in the realm of continuum mechanics, by means of a suitable extension to the hydrodynamic equations of active nematic liquid crystals. These have been successfully used in the past decade to describe a variety of active fluids, typically of biological origin, consisting of self or mutually propelled apolar building blocks, such as *in vitro* suspensions of microtubules and kinesin [20, 36–42], microswimmers [43] and cellular monolayers [44]. Attempts to describe sessile bacteria, in the language of nematic liquid crystals, have been recently made [13, 42]. Here we introduce a comprehensive hydrodynamic framework, incorporating the density effects described in the previous section and, for the first time in our knowledge, account for the deviatoric active stresses in the colonization dynamics.

An expanding bacterial colony can be described in terms of the material fields ρ , \mathbf{v} and \mathbf{Q} , representing respectively the cell density, velocity, and the nematic order. The latter is represented via the two-dimensional tensor field $\mathbf{Q} = S(\mathbf{n} \mathbf{n} - \mathbf{I}/2)$ [46], where $0 \leq S \leq 1$ is an order parameter quantifying the local nematic order of the cells. The dynamics of these fields is then governed by the following hydrodynamic equations [34]:

$$\partial_t \rho + \nabla \cdot (\rho \mathbf{v}) = k_g \rho + D \nabla^2 \rho, \quad (11a)$$

$$\partial_t (\rho \mathbf{v}) + \nabla \cdot (\rho \mathbf{v} \mathbf{v}) = \nabla \cdot \boldsymbol{\sigma} - \xi \rho \mathbf{v}, \quad (11b)$$

$$\partial_t \mathbf{Q} + \mathbf{v} \cdot \nabla \mathbf{Q} = \lambda S \mathbf{u} + [\mathbf{Q}, \boldsymbol{\omega}] + \gamma^{-1} \mathbf{H}, \quad (11c)$$

with $[\cdot, \cdot]$ the anti-commutator. Eq. (11a), describes an exponential growth of the colony total mass at rate k_g (proportional to the length extension rate g used in Sec. I). As the cells duplicate, they are transported across the

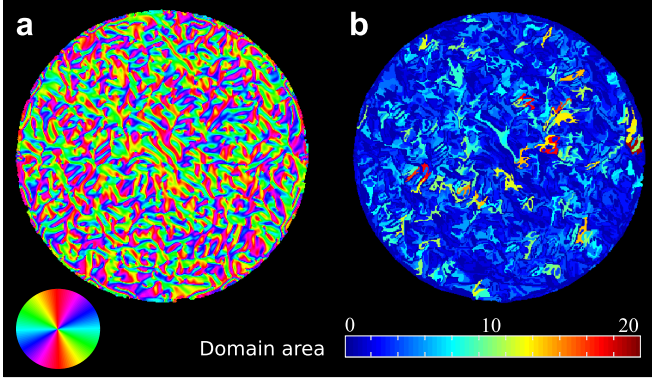


FIG. 6. **Continuous Model.** (a) Snapshot of a typical configuration obtained from a numerical integration of Eqs. (11). Displayed here is the angle between the nematic director and the x -axis, colored using the same color scheme as in Fig. 1. (b) The nematic director is coarse-grained and a connected component labelling algorithm is used to identify domains. This is displayed here with each domain coloured by its size.

colony by convective currents. An additional diffusive term, with D a small diffusion coefficient, is introduced for regularization. The cells momentum density $\rho \mathbf{v}$ is subject to the internal stresses $\boldsymbol{\sigma}$ as well as the frictional force $-\xi \rho \mathbf{v}$. The former can, in turn, be expressed as

$$\boldsymbol{\sigma} = -p\mathbf{I} + \alpha\mathbf{Q} - \lambda S\mathbf{H} + [\mathbf{Q}, \mathbf{H}], \quad (12)$$

where the first two terms represent, as in Eq. (5), the isotropic pressure and extensile active stress introduced by the cell growth. The remaining terms describe the elastic stresses in the colony arising due to the passive aligning interactions between the cells. The tensor field \mathbf{H} in Eqs.(11c) and (12), can be defined starting from the Landau-de Gennes free energy density:

$$f_{\text{LdG}} = \frac{1}{2}L_1|\nabla\mathbf{Q}|^2 + \frac{1}{2}A_2\text{tr}\mathbf{Q}^2 + \frac{1}{4}A_4(\text{tr}\mathbf{Q}^2)^2, \quad (13)$$

as $\mathbf{H} = -\delta/\delta\mathbf{Q} \int dA f_{\text{LdG}}$. Here $L_1 \sim k_F$ is an orientational stiffness, while the functions A_2 and A_4 set the boundary between the isotropic ($S = 0$) and nematic ($S > 0$) phase. At equilibrium, $\mathbf{H} = \mathbf{0}$ and $S = \sqrt{-2A_2/A_4}$. In our system of growing cells, orientational order is driven uniquely by the steric repulsion and the system transitions to a nematic phase for large enough densities. We set $A_2 = A_0(\rho^* - \rho)$ and $A_4 = A_0\rho$, so that the system has an equilibrium order parameter $S = \sqrt{1 - \rho^*/\rho}$, with a critical density ρ^* , hence the colony is disordered for densities $\rho < \rho^*$ and nematic for $\rho > \rho^*$. Finally, the nematic director relaxes toward the minimum of the Landau-de Gennes energy (13) while rotating as a consequence of the internal motion of the cells. This effect is embodied in the first two terms of Eq. (11c), with $u_{ij} = (\partial_i v_j + \partial_j v_i - \delta_{ij} \nabla \cdot \mathbf{v})/2$ and $\omega_{ij} = (\partial_i v_j - \partial_j v_i)/2$ representing strain rate and the vorticity tensor, respectively, and λ the flow-alignment parameter [34].

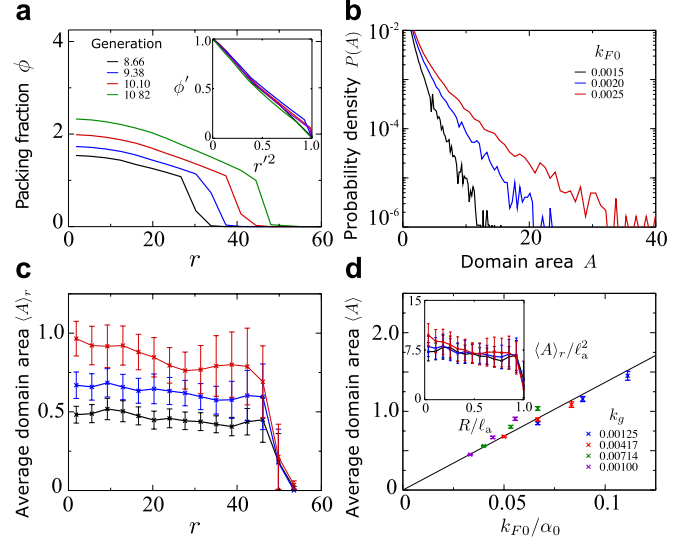


FIG. 7. **Geometrical properties of continuous colonies.** (a) Radial distribution of packing fraction ($\phi = \rho/\rho_c$) for colonies of different ages, given by their generation. Similar to the hard-rod model, the inset shows all curves collapse to a single line when ϕ and r are rescaled by $\phi' = [\phi(r) - \phi(R)]/(\phi(0) - \phi(R))$ and $r' = r/R$. (b) Probability density of the domain area, $P(A)$, for various values of the orientational stiffness k_{F0} . (c) The average domain area at a distance r from the center of the colony. As in the hard-rod model, the typical domain area is uniform across the colony. (d) The average domain area for a colony scales linearly with the squared active length scale $\ell_a^2 = k_F/|\alpha|$. The inset shows that the radial distribution of domain areas can be rescaled by the squared active length scale to the same value. In the continuous model we use $l = 1/\sqrt{\rho_c}$ as our units of length, our units of time are $t_g = \log(2)/k_g$ which gives the doubling time which we interpret as the time per generation.

Now, consistent with the results of our hard-rod model presented in Sec. IB, we encode a specific density dependence in the quantities p , α and k_F . Introducing the packing fraction $\phi = \rho/\rho_c$, where ρ_c is the density at which cells become close packed and start to transmit stress. In the following we assume $\rho_c > \rho^*$, to reflect the earlier observation that at very low density (i.e. at the boundary of the colony) the contact forces tend to reorientate cells rather than compressing them. Based on these considerations, we set:

$$p = p_0(\phi - 1), \quad \alpha = -\alpha_0(\phi - 1), \quad k_F = k_{F0}(\phi - 1),$$

where p_0 , α_0 and k_{F0} are positive constants. Furthermore, we take $\alpha_0 \sim k_g$ and keep p_0 constant based on the results summarized in Fig 5c. Eqs. (11) have been numerically solved using a finite difference approach on a 351×351 collocated grid. Fig 6a (inset) shows a typical configuration obtained for sufficiently large growth rates. As for our hard-rod model, these consist of an ensemble of randomly oriented nematic domains, whose characteristic area remains uniform in the bulk of the colony. In order to make a quantitative comparison between our discrete

and continuous model, we reconstruct the geometrical properties of the micro-domains based on the following criterion. Given the orientation $\theta = \arctan(Q_{xy}/Q_{xx})$ of the nematic director, we define Θ as the coarse-grained θ field in which all values are sorted into bins; e.g. $2(n-1)\pi/m \leq \theta < 2n\pi/m \implies \Theta = (2n-1)\pi/m$ for $n = 1, 2 \dots m$ (n and m both integers). This divides the colony into domains that can then be identified by labeling the connected components of the resulting two-dimensional matrix. We use a value of $m = 6$ here to reflect a typical θ change between two boundaries in the hard-rod model. Fig. 6b shows the sizes of domains reconstructed from the colony shown in Fig. 6a.

Fig. 7 summarizes the result obtained from a numerical integration of Eqs. (11). As for the hard-rod model, the density decreases monotonically from the center of the colony, consistent with the quadratic law given by Eq. (3) (Fig. 7a). Here we demonstrate that such a property originates from the interplay between growth-induced pressure and drag. Under this hypothesis and assuming low Reynolds number, from Eq. (11c) one can approximate the momentum density in the Darcy-like form $\rho \mathbf{v} = -\mu \nabla \rho$, where $\mu = p_0/(\xi \rho_c)$ is a mobility coefficient. Using this relation in Eq. (11a), yields the following moving boundary value problem for the colony density:

$$\partial_t \rho = \mu \nabla^2 \rho + k_g \rho, \quad |\mathbf{r}| < |\mathbf{R}|, \quad (14a)$$

$$\rho(\mathbf{R}, t) = \rho_c, \quad (14b)$$

$$\dot{\mathbf{R}} = -\mu \rho^{-1} \nabla \rho|_{\mathbf{r}=\mathbf{R}}, \quad (14c)$$

where we have indicated with \mathbf{R} the position of the boundary of the colony and with $\dot{\mathbf{R}} = \mathbf{v}(\mathbf{R})$ its velocity. Because of the circular symmetry of the colony at long times, $\mathbf{R} = R\hat{\mathbf{r}}$ and Eqs. (14) reduces to a Stefan problem with one spatial and one temporal variable [47]. An analytical solution of Eqs. (14) can be found in the long time limit. In this regime, $\rho(0, t) \gg \rho_c$ and $R \gg \sqrt{\mu/\kappa_g}$, this being the characteristic length scale associated with Eq. (14a). Thus, taking $\rho_c \rightarrow 0$, $R \rightarrow \infty$ and choosing $\rho(\mathbf{r}, 0) = M\delta(\mathbf{r})$, with M the mass of a single bacterium, as initial configuration, yields:

$$\rho(r, t) = \frac{M}{4\pi\mu t} \exp\left(k_g t - \frac{r^2}{4\mu t}\right). \quad (15)$$

Thus, in agreement with Eq. (3), we have that:

$$\frac{\rho(r, t)}{\rho(0, t)} \approx 1 - \left(\frac{r}{R}\right)^2, \quad (16)$$

where, consistently with Eq. (14c), we have taken $R = 2\sqrt{\mu t}$. For generic ρ_c and R values, Eqs. (14) becomes analytically intractable, nonetheless our numerical simulations (Fig. 7a) indicate that even the short time dynamics of the density ρ is ultimately dominated by a similar competition between growth and drag.

The geometrical properties of the nematic micro-domains are summarized in Figs. 7b-d and show excellent agreement with the hard-rod model. The area of the domains is exponentially distributed (Fig. 7b) and its average $\langle A \rangle_r$ is uniform across the colony (Fig. 7c) and proportional to the squared active length scale as demanded by Eq. (10) (Fig. 7d). The agreement between our discrete and continuous model, not only validates our interpretation of the results presented in Sec. I, but further provides an efficient method to simulate growing bacterial colonies. Unlike discrete particles methods (including that used in Sec. I), our hydrodynamic approach does not suffer from the prohibitive slow-down caused by the exponential increase in the particles number and can be naturally generalized to other geometries and boundary conditions.

III. Discussion and Conclusions

Sessile bacteria communities have the extraordinary ability of colonizing a variety of surfaces, even in the presence of non-optimal environmental conditions. Such a process typically starts from few or even a single cell, that elongate and eventually divide at a constant rate, and give rise to highly complex two-dimensional and three-dimensional structures consisting of tightly packed and partially ordered cells. Colonies originating from a single bacterium, initially develops in the form of a flat and circularly symmetric monolayer and, after reaching a critical population, invade the three-dimensional space forming stacks of concentric disk-shaped layers [15, 19]. While in the monolayer form, bacterial colonies exhibit prominent nematic order, this, however, does not propagate across the colony, and remains confined into a set of microscopic domains of co-aligned cells. Using discrete and continuous modeling, we have demonstrated that these domains originates from the interplay of two competing forces. On the one hand, the steric forces between neighboring cells favor alignment. On the other hand, the extensile active stresses due to growth tend to distort the system and disrupt the local orientational order. This results into an exponential distribution of the domains area, with a characteristic length scale $\ell_a = \sqrt{k_F/|\alpha|}$, where k_F is the orientational stiffness of the nematic domains and α the magnitude of the deviatoric active stress. As it has been already observed in planktonic bacteria [35], we expect that confining a growing colony into a restricted environment could substantially alter the spatial organization of the micro-domains, depending on how the confinement length scale compares with the inherent length scale ℓ_a .

Despite cell morphology being one of the most well-documented phenotypic traits of microorganisms, its role as a functional trait in microbial ecology and evolution, has received only a scant attention [48]. The spontaneous creation of micro-domains during the initial stages of colony growth presents a remarkable setting, one in which *non-motile* bacterial cells collectively lead to *emergent*

motility within the colony, as visualized in the chaotic fracture and coarsening dynamics of the nematic domains. Consequently, this interplay between growth-induced stresses and phenotypic stiffness of the participating cells, introduces a novel angle to the transport and material attributes of such biologically active matter. Future studies on emergent motility within colonies of non-motile cells, both experiments and theory, are expected contribute toward a comprehensive biomechanical picture, highlighting the activity-driven cell-cell communications that precede biofilm formation. Finally, the

results presented here are general, and can be extended beyond bacterial communities, for instance, to also study mammalian cells, many of which exist as non-motile elongated phenotypes [49].

Acknowledgments

ZY, DJGP and LG are supported by The Netherlands Organization for Scientific Research (NWO/OCW) as part of the Frontiers of Nanoscience program. AS was supported by Human Frontier Science Program Cross Disciplinary Fellowship (LT000993/2014-C), and thanks Jennifer Nguyen and Roman Stocker for discussions.

-
- [1] D. McDougald, S. A. Rice, N. Barraud, P. D. Steinberg, S. Kjelleberg, *Should we stay or should we go: mechanisms and ecological consequences for biofilm dispersal*, *Nat. Rev. Microbiol.* **10**, 39 (2012).
 - [2] B. Rosan and R. J. Lamont, *Dental plaque formation*, *Microbes and Infection* **2**, 1599 (2000).
 - [3] J. B. Kaplan, *Biofilm dispersal: mechanisms, clinical implications, and potential therapeutic uses*, *J. Dent. Res.* **89**, 205 (2010).
 - [4] J. W. Costerton, P. S. Stewart, E. P. Greenberg, *Bacterial biofilms: a common cause of persistent infections*, *Science* **284**, 1318 (1999).
 - [5] J. W. Costerton, Z. Lewandowski, D. E. Caldwell, D. R. Korber, H. M. Lappin-Scott, *Microbial biofilms*, *Annu. Rev. Microbiol.* **49**, 711 (1995).
 - [6] A. Persat, C. D. Nadell, M. K. Kim, F. Ingremeau, A. Siryaporn, K. Drescher, N. S. Wingreen, B. L. Bassler, Z. Gitai, and H. A. Stone, *The Mechanical world of bacteria*, *Cell* **161**, 988 (2015).
 - [7] J. A. Shapiro, *Bacteria as multicellular organisms*, *Sci. Am.* **256**, 82 (1988).
 - [8] J. A. Shapiro, *Thinking about bacterial populations as multicellular organisms*, *Annu. Rev. Microbiol.* **52**, 81 (1998).
 - [9] B. J. Crespi, *The evolution of social behavior in microorganisms*, *Trends in Ecology and Evolution* **16**, 178 (2001).
 - [10] B. D. Hoffman, C. Grashoff, M. A. Schwartz, *Dynamic molecular processes mediate cellular mechanotransduction*, *Nature* **475**, 316 (2001).
 - [11] D. M. Morris and G. J. Jensen, *Toward a biomechanical understanding of whole bacterial cells*, *Annu. Rev. Biochem.* **77**, 583 (2008).
 - [12] H. Cho, H. Jönsson, K. Campbell, P. Melke, J. W. Williams, B. Jedynak, A. M. Stevens, A. Groisman, A. Levchenko, *Self-Organization in high-density bacterial colonies: Efficient crowd control*, *PLoS Biol.* **5**, e302 (2007).
 - [13] D. Volfson, S. Cookson, J. Hasty, L. S. Tsimring, *Biomechanical ordering of dense cell populations*, *Proc. Natl. Acad. Sci. U. S. A.* **105**, 15346 (2008).
 - [14] D. Boyer, W. Mather, O. Mondragón-Palomino, S. Orozco-Fuentes, T. Danino, J. Hasty, L. S. Tsimring, *Buckling instability in ordered bacterial colonies*, *Phys. Biol.* **8**, 026008 (2011).
 - [15] P.-T. Su, C.-T. Liao, J.-R. Roan, S.-H. Wang, A. Chiou, W.-J. Syu, *Bacterial colony from two-dimensional division to three-dimensional development*, *PLoS ONE* **7**, e48098 (2012).
 - [16] S. Orozco-Fuentes, D. Boyer *Order, intermittency, and pressure fluctuations in a system of proliferating rods*, *Phys. Rev. E* **88**, 012715 (2013).
 - [17] T. J. Rudge, F. Federici, P. J. Steiner, A. Kan, J. Haseloff, *Cell polarity-driven instability generates self-organized, fractal patterning of cell layers*, *ACS Synth. Biol.* **2**, 705 (2013).
 - [18] F. D. C. Farrell, O. Hallatschek, D. Marenduzzo, B. Waclaw, *Mechanically driven growth of quasi-two-dimensional microbial colonies*, *Phys. Rev. Lett.* **111**, 0168101 (2013).
 - [19] M. A. A. Grant, B. Waclaw, R. J. Allen, P. Cicuta, *The role of mechanical forces in the planar-to-bulk transition in growing Escherichia coli microcolonies*, *J. R. Soc. Interface* **11**, 20140400 (2014).
 - [20] L. Gioni *The geometry and topology of turbulence in active nematics*, *Phys. Rev. X* **5**, 031003 (2015).
 - [21] Y. Sumino, K. H. Nagai, Y. Shitaka, D. Tanaka, K. Yoshikawa, H. Chaté, K. Oiwa, *Large-scale vortex lattice emerging from collectively moving microtubules*, *Nature* **483**, 448 (2012).
 - [22] T. Sanchez, D. N. Chen, S. J. DeCamp, M. Heymann, Z. Dogic, *Spontaneous motion in hierarchically assembled active matter*, *Nature* **491**, 431 (2012).
 - [23] S. J. DeCamp, G. S. Redner, A. Baskaran, M. F. Hagan, Z. Dogic, *Orientational order of motile defects in active nematics*, *Nat. Mater.* **14**, 1110 (2015).
 - [24] P. Guillamat, J. Ignés-Mullol, F. Sagués, *Control of active liquid crystals with a magnetic field*, *Proc. Natl. Acad. Sci. U.S.A.* **113**, 5498 (2016).
 - [25] P. Kumar, A. Libchaber, *Pressure and temperature dependence of growth and morphology of Escherichia coli: Experiments and stochastic model*, *Biophys. J.* **105**, 783 (2013).
 - [26] P. M. Chaikin, T. C. Lubensky, *Principles of condensed matter physics*. (Cambridge University Press, Cambridge 1995).
 - [27] L. D. Landau, E. M. Lifshitz, *Theory of elasticity* 3rd ed. (Butterworth-Heinemann, Oxford).
 - [28] T. J. Pedley, J. O. Kessler, *Hydrodynamic phenomena in suspensions of swimming microorganisms*, *Annu. Rev. Fluid Mech.* **24**, 313 (1992).

- [29] Y. Hatwalne, S. Ramaswamy, M. Rao, R. A. Simha, *Rheology of active-particle suspensions*, *Phys. Rev. Lett.* **92**, 118101 (2004).
- [30] R. Voituriez, J.-F. Joanny, J. Prost, *Spontaneous flow transition in active polar gels* *Europhys. Lett.* **70**, 404 (2005).
- [31] D. Marenduzzo, E. Orlandini, M. E. Cates, and J. M. Yeomans, *Steady-state hydrodynamic instabilities of active liquid crystals: Hybrid lattice Boltzmann simulations*, *Phys. Rev. E* **76**, 031921 (2007).
- [32] S. A. Edwards, J. M. Yeomans, *Spontaneous flow states in active nematics: a unified picture* *Europhys. Lett.* **85**, 18008 (2009).
- [33] L. Giomi, L. Mahadevan, B. Chakraborty, M. F. Hagan, *Excitable patterns in active nematics*, *Phys. Rev. Lett.* **106**, 218101 (2011).
- [34] L. Giomi, L. Mahadevan, B. Chakraborty, M. F. Hagan, *Banding, excitability and chaos in active nematic suspensions* *Nonlinearity* **25**, 2245 (2012).
- [35] H. Wioland, E. Lushi, R. E. Goldstein, *Directed collective motion of bacteria under channel confinement*, *New J. Phys.* **18** 075002 (2016).
- [36] A. Ahmadi, T. B. Liverpool, M. C. Marchetti, *Nematic and polar order in active filament solutions*, *Phys. Rev. E* **72**, 060901(R) (2005).
- [37] A. Ahmadi, M. C. Marchetti, T. B. Liverpool, *Hydrodynamics of isotropic and liquid crystalline active polymer solutions*, *Phys. Rev. E* **74**, 061913 (2006).
- [38] T. B. Liverpool and M. C. Marchetti, *Hydrodynamics and rheology of active polar filaments*, in *Cell Motility*, P. Lenz ed. (Springer, New York, 2007).
- [39] *Defect annihilation and proliferation in active nematics*, L. Giomi, M. J. Bowick, X. Ma and M. C. Marchetti *Phys. Rev. Lett.* **110**, 228101 (2013).
- [40] *Defect dynamics in active nematics*, L. Giomi, M. J. Bowick, P. Mishra, R. Sknepnek and M. C. Marchetti *Phil. Trans. R. Soc. A* **372**, 20130365 (2014).
- [41] S. P. Thampi, . Golestanian, J. M. Yeomans, *Velocity correlations in an active nematic*, *Phys. Rev. Lett.* **111**, 118101 (2013).
- [42] A. Doostmohammadi, M. F. Adamer, S. P. Thampi, J. M. Yeomans, *Stabilization of active matter by flow-vortex lattices and defect ordering*, *Nat. Commun.* **7**, 10557 (2016).
- [43] A. W. C. Lau, and T. C. Lubensky, *Fluctuating hydrodynamics and microrheology of a dilute suspension of swimming bacteria*, *Phys. Rev. E* **80**, 011917 (2009).
- [44] A. Doostmohammadi, S. P. Thampi, T. B. Saw, C. T. Lim, B. Ladoux, J. M. Yeomans, *Celebrating Soft Matter's 10th Anniversary: Cell division: a source of active stress in cellular monolayers*, *Soft Matter* **11**, 7328 (2015).
- [45] A. Doostmohammadi, S. P. Thampi, J. M. Yeomans, *Defect-mediated morphologies in growing cell colonies*, *Phys. Rev. Lett.* **117**, 048102 (2016).
- [46] P. G. de Gennes, J. Prost, *The Physics of Liquid Crystals* 2nd edn. (Oxford University Press, Oxford 1993).
- [47] J. Ockendon, S. Howison, A. Lacey, A. Movchan, *Applied partial differential equations* (Oxford University Press, Oxford, 2003).
- [48] W. P. J. Smith, Y. Davit, J. M. Osbornec, W. Kim, K. R. Fosterd, J. M. Pitt-Francis, *Cell morphology drives spatial patterning in microbial communities*, *Proc. Natl. Acad. Sci. U. S. A.* **E280-E286** **114**, (2016).
- [49] G. Duclos, C. Erlenkmpfer, J.-F. Joanny, P. Silberzan, *Topological defects in confined populations of spindle-shaped cells*, *Nat. Phys.* **13**, 58-62 (2017).